

High Intensity ultrashort laser pulses and their applications at IPEN

Ricardo Elgul Samad
IPEN – CNEN/SP
São Paulo, SP, Brazil
resamad@gmail.com

Edison Puig Maldonado
IEE – ITA
São José dos Campos, SP, Brazil
puig@ita.br

Wagner de Rossi
IPEN – CNEN/SP
São Paulo, SP, Brazil
wderossi@ipen.br

Nilson Dias Vieira Junior
IPEN – CNEN/SP
São Paulo, SP, Brazil
nilsondiasvieirajr@gmail.com

Abstract—Ultrashort laser pulses interact with matter in unique, nonselective ways, due to electronic direct excitation in an ultrafast time scale. Additionally, these pulses can cover peak powers from kW to PW, allowing its use to induce from nonlinear optics up to relativistic phenomena. Here we present a quick overview of the important processes induced in matter by high-intensity ultrashort pulses, and describe results obtained in our laboratory, including our most recent goal of accelerating electrons with ultrashort pulses for practical applications.

Keywords—ultrashort laser pulses, high intensity lasers, laser induced plasma, LWFA

I. INTRODUCTION

High intensity femtosecond (fs) lasers appeared in the second half of the 1980 decade as a consequence of the discovery of broadband gain media such as Ti:sapphire [1], and the introduction of the Chirped Pulse Amplification (CPA) technique [2], in which a pulse is temporally stretched, amplified and compressed. Nowadays ultrafast technology based on solid state and fiber lasers [3-5], and diode laser pumping is ubiquitous in optical laboratories around the world. Peak intensities range from a few kW at high repetition rates ($\sim 10^8$ Hz), up to a few PW and sub-Hz repetition rates in national facilities [6], opening new avenues for ultrafast science and applications. These laser systems can also directly produce pulses with durations under 5 fs, close to an optical cycle, and generate few tens of attosecond (10^{-18} s) pulses, the shortest events ever created by mankind, giving birth to zeptosecond (10^{-21} s) physics [7] and allowing deep studies in quantum physics.

Ultrashort pulses (loosely defined as those shorter than 1 picosecond) spanning peak powers over more than 12 orders of magnitude have become a versatile tool to induce nonlinear phenomena aiming to study, modify and characterize all kinds of materials and states of matter. These capabilities derive from the ultrafast interaction between the electromagnetic field and matter, which distinguishes this kind of laser from all others.

In the time frame of ultrashort pulses, the predominant interaction with matter occurs by electron excitation, and several processes take place with increasing intensity: linear response, followed by nonlinear excitation, field-induced ionization, collisional ionization, plasma formation and free electrons acceleration, phenomena that are almost independent of the material, due to the short time of interaction. In the cases in which ionization occurs, the after-pulse evolution usually happens by electrostatic interactions, involving the relaxation of the electrons energy to and between neighboring atoms, resulting in light emission in plasmas and ultrafast heating in solids. The later usually leads to material modifications and phase explosions that ablate the

This work was supported by FAPESP, SAE and CNPq.

irradiated area. The interaction of higher intensity pulses with plasmas can drive electrons into high kinetic energy trajectories that can result in the emission of shorter wavelengths than those of the exciting field, into the x-ray region, and even the creation of spatial charge distributions that accelerate particles.

At the High Intensity Ultrashort Pulses Lasers Laboratory at IPEN we routinely generate femtosecond pulses with intensities of 100 TW/cm^2 and above. In this work we describe results obtained by our group using ultrashort pulses from Ti:sapphire laser systems covering the induction of nonlinear phenomena, the creation of color centers in crystals, glasses and polymers, the inscription of waveguides and the creation of surface structures that can range from the colorization of metals to the manufacture of microfluidic circuits, as well as the *in vivo* removal of burned tissue. The pulses can also be used to study how defects pileup during the etching of solids by superimposing pulses, and how the ablation process is affected by this incubation. At higher intensities, the pulses can modify materials, like the transformation of graphite into diamond by shockwaves generated during ablation; the shockwaves are a product of an evolving underdense plasma that generates local high temperatures and pressures. Additionally, the *in situ* materials characterization is possible by spectroscopic measurements of the plasma elements atomic lines. Finally, we show results on the production of coherent vacuum ultraviolet radiation and the first results in our research of electron acceleration by ultrashort laser pulses.

II. ULTRASHORT PULSES INTERACTION WITH MATTER

When light interacts with matter, the main response comes from the electrons, which are accelerated by its electric field, E , and can be quantified by the material electronic polarization, P [8]. For low intensity fields, P is a linear function of the excitation and originates common phenomena like absorption, refraction, reflection, transmission, among others [8]. As the light intensity increases the system enters the perturbative nonlinear regime, and the polarization is no longer a linear response to the exciting electric field, and can be expanded as a power series of E [9]:

$$P = \chi^{(1)}E + \chi^{(2)}E^2 + \chi^{(3)}E^3 + \dots, \quad (1)$$

where $\chi^{(n)}$ is the material n -th order polarizability, and it was assumed that the field is linearly polarized and the electronic polarization oscillates in the same direction. From Eq. (1) follows that, for a sinusoidal excitation $E = E_0 \cos(\omega t)$, the electronic polarization will oscillate at multiples of the exciting frequency, ω , radiating light at these harmonics [9]. For more intense light, the matter response cannot be described as a power series, entering the non-perturbative regime [10], and from there into the ionization domain. The ionization starts as a multiphoton process, in which n photons are absorbed, promoting the electron from its level in potential

well into the continuum, as outlined in Fig. 1a; as the intensity increases, the exciting field potential (red in Fig. 1b) distorts the potential well, creating conditions for the electron to tunnel across the lowered barrier. The Keldysh parameter [11], which compares the tunneling time with the distorted potential duration, describes the transition from the multiphotonic to the tunneling regime.

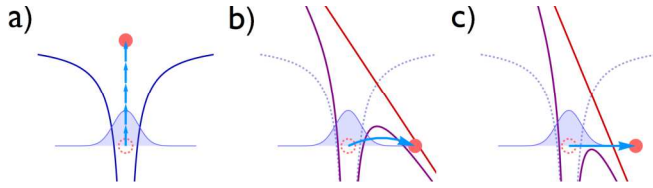


Fig. 1. Ionization processes: a) multiphotonic; b) tunneling; c) barrier suppression.

At even higher field intensities, the potential well is severely distorted, lowering the barrier to below the electron fundamental state potential (Fig. 1c), so it escapes the atom by the process known as barrier suppression ionization (BSI) [12]. The ionization process, independently of the details, occurs in the leading edge of an ultrashort pulse, and when it takes place in a solid, the freed electrons can be accelerated (heated) [13] by the remaining of the pulse, creating more free electrons by collisional (avalanche) ionization [14, 15]. The free electron density, n_e , grows exponentially to quickly reach the critical plasma density, for which the laser frequency equals the plasma frequency, $\omega_p = (e/\epsilon_0)^{1/2} \times (n_e/m_e)^{1/2}$, preventing the laser propagation through the material [8]. For $\lambda = 800$ nm, this critical density is 1.7×10^{21} e/cm³, representing on the order of 1 free electron per material atom, strongly heated by the laser field [13]. After the passage of the pulse, the electrons relax their energy to the material atoms and ions, and breakdown occurs [16] by a combination of the material ions Coulomb explosion [17] and phase explosion resulting from excess energy delivered by the electrons [18-20]. This ablation can be regarded as almost non-thermal [21], since the electrons heating occurs in the femtosecond scale, much shorter than the material typical phonon period and heat conduction time [22], and the ejected material carries away almost all the remaining energy. As a consequence of these explosions, ablation occurs in the material, forming a high-temperature plasma that is ejected [23]. The controlled ablation is spatially limited and can be used to precisely machine any kind of material (due to the nonselective interaction rising from the electrons response) preserving the bulk properties, which are not modified due to the negligible thermal interaction, with the additional advantage of a nearly non-existing heat affected zone. Also, the ejected plasma can be used to characterize the material elemental composition in a technique known as Laser Induced Breakdown Spectroscopy [24]. This technique measures the spectrum emitted by the plasma, which contains atomic and ionic emission lines originated by the electrons recombination, seated on the top of the plasma thermal spectrum. When ultrashort pulses are used, in what became known as fs-LIBS [25], the small amount of pulse energy decreases the thermal background spectrum, highlighting the atomic emission lines. Also, due to the ultrashort pulse high intensities, the atoms can be ionized several times, reaching high charge states.

When ultrashort pulses ionize a gas, at $\sim 10^{14}$ - 10^{15} W/cm² intensities, a freed electron can be accelerated away from its parent ion by the laser electric field. Since the field is

sinusoidal, the electron can be brought back to the ion and recombine, emitting a photon whose energy is the electron kinetic energy added to the atom ionization energy. This process is described by the three-step model [26, 27]. When this emission occurs periodically at each half-optical cycle, odd harmonics of the exciting field are emitted [28], extending up to the keV range depending on the pulse intensity, wavelength and gas used [29]. This technique is known as High Harmonic Generation (HHG), and nowadays is widely used to generate coherent radiation in the extreme UV and soft x ray spectrum [30]. Decreasing the exciting pulse duration to a few optical cycles washes away the harmonic structure from the emission spectrum, providing bandwidth that can be compressed to attosecond pulses [27, 31].

The electrons oscillating in the laser pulse field are also subjected to the ponderomotive force, which is a nonlinear force that a charged particle experiences in an inhomogeneous oscillating electromagnetic field, expressed by [32]:

$$\mathbf{F}_p = -e^2/(4m_e\omega^2) \nabla E^2, \quad (2)$$

where e and m_e are the electron charge and mass, respectively. The ponderomotive force is proportional to the laser pulse time averaged intensity gradient, and it moves the electrons towards the weaker field regions, as represented in Fig. 2.

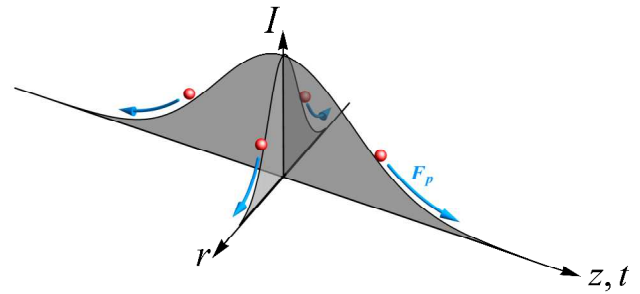


Fig. 2. Representation of the ponderomotive force that a Gaussian pulse propagating in the z direction exerts on the electrons (red dots), moving them away from the intensity peak.

When the laser intensity reaches $\sim 10^{18}$ W/cm², the electrons accelerated by the pulse electric field approach the speed of light, the Lorentz force originated by the interaction with the pulse magnetic field becomes comparable to the electric force, and the electrons are said to be in the relativistic regime [33]. Also, at these intensities the ponderomotive force grows comparable to the other electromagnetic forces and expels the electrons from the center of the pulse due to its temporal and spatial gradients, as shown in Fig. 2. This dynamics builds up the positive ions concentration close to the longitudinal axis (since they do not move during the pulse duration), creating ion cavities (or bubbles) that follow the pulse [34], forming a wake. The (almost) periodic charge distribution originated, with ions at the center of the bubbles and electrons concentrated at its extremities on the axis, originate electric fields that can reach 100 GV/m [35]; when an electron is trapped in one of these cavities it can be strongly accelerated, and if it matches the wake speed, this acceleration continues for a few centimeters and can rise the electron energy up to a few GeV [36]. Due to the formed wake that follows the pulse, this technique is known as Laser Wakefield Acceleration (LWFA) [37].

The ultrafast, laser-induced heterogeneities in the electron density (the nonlinear wake) lead to ponderomotive nonlinear phenomena. On the other hand, the electron increases its mass in the relativistic regime, and nonlinear relativistic phenomena also start to manifest. Relativistic self-focusing occurs when the index of refraction has a radial maximum on-axis caused by the peak in the laser intensity [34]. The focalization caused by this nonlinear effect can cause the spatial collapse of the pulse to its diffraction limit, greatly increasing its intensity, originating phenomena that would not be attainable with the pulse original intensity.

III. ULTRASHORT PULSES LASER SYSTEMS AT IPEN

At the Center for Lasers and Applications (CLA) at IPEN we have three high intensity CPA systems. The first one (Odin, from Quantronix) is a Ti:sapphire based main oscillator and amplifier, and generates 50 fs, < 1 mJ pulses centered at 800 nm, at 1 kHz repetition rate. This system was modified to allow the extraction of the amplified, uncompressed pulses, for further amplification. A pulsed lamp-pumped Cr:LiSAF cavity was developed and built, containing optical filters [38, 39] that matched the lamps emission to the gain medium absorption spectrum. This spectral selection and the lamps emission duration equaling the gain medium lifetime decreased the heat generation in the crystal by absorption and Stokes-shift, avoiding the luminescence quenching that occurs at $\sim 70^\circ\text{C}$ in this crystal, keeping a high gain up to 30 Hz repetition rate. When operating as a laser, this pumping cavity could generate 2 J pulses at 15 Hz, with 30 W average power [39], and when used to amplify the uncompressed pulses in a 4-pass multipass configuration, a gain over 100 was obtained [40], allowing the generation of 0.5 TW pulses after compression, the highest peak power in Brazil at that time.

The second system is also Ti:sapphire based (main oscillator Rainbow, amplifier Femtopower Compact Pro CE-Phase HP/HR, both from Femtolasers), generating 25 fs, < 800 μJ pulses centered at 785 nm, at 4 kHz. The pulses can be injected in a hollow fiber with neon at high pressure, which widens their spectrum, and compressed down to 5 fs with chirped mirrors [41]. These pulses are CEP stabilized down to a few tens of mrad [42], which is important for experiments with pulses this short.

The third system, also Ti:sapphire based, is similar to the second one, being modified to increase the repetition rate to 10 kHz with 200 μJ of maximum energy in 25 fs pulses (main oscillator Element, Amplifier Femtopower, from Femtolasers). The output of this system is integrated into a high-precision machining station, dedicated to ultrashort pulses micromachining.

All the results present in this work were obtained in our laboratories, in one of the three systems described above.

IV. RESULTS

A. Self-Phase Modulation in waveguides

At low intensities, around $10^9 - 10^{10}\text{ W/cm}^2$, perturbative phenomena, described by Eq. (1) occur. As an example, from this equation follows [9] that the total refractive index of a material has a nonlinear component proportional to $n_2 \sim \text{Re}[\chi^{(3)}]$ and to the intensity of the light in the material. In the self-phase modulation (SPM) [43] phenomenon, a laser pulse can displace its carrier frequency ω by:

$$\Delta\omega = -2(\pi/\lambda) \ln_2 I'(t-t_0), \quad (2)$$

where l is the distance traveled in the material, I' is the pulse temporal derivative, and t_0 is its peak time. Eq. (2) shows that the pulse leading edge has its frequency shifted to red, while the trailing edge is blue-shifted, widening its spectrum [44]. We have used 23 fs pulses, with 40 nm of bandwidth, to determine the nonlinear refractive index of Ta₂O₅ pedestal waveguides [45], measuring the widening dependence on the pulses peak power, as shown in Fig. 3. As the power increases, the spectrum widens up to $\sim 80\text{ nm}$, providing a nonlinear refractive index $n_2 = 5.8 \times 10^{-15}\text{ m}^2/\text{W}$.

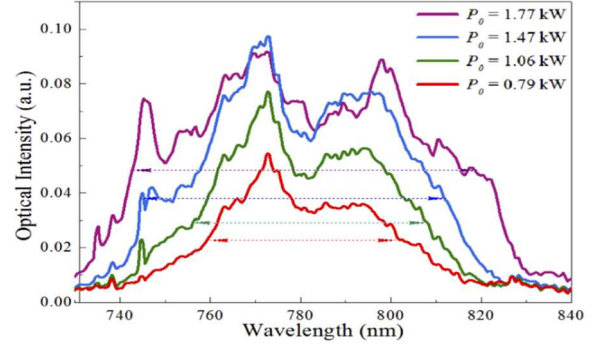


Fig. 3. Optical spectra widening due to SPM at the waveguide output.

B. Creation of Defects and Waveguides

Increasing the pulse intensity to $\sim 10^{12} - 10^{13}\text{ W/cm}^2$ starts creating free electrons in solids by either multiphotonic or tunneling ionization, but these intensities are not enough to promote a significant increase in the free electrons' density by impact ionization. Nevertheless, free electrons are created, leaving neutral atoms behind, which can migrate away from their equilibrium sites in solids, creating vacancies and defects. When a vacancy captures an electron, color centers are formed [46-48], changing the absorption and emission properties of the material, the same occurring for defects. The Kramers-Kronig relations establish that a change in a material absorption will produce a variation in its refractive index [49], and if the defects are created with spatial control, waveguides can be written in a material [50].

C. Ablation, Incubation and Material Processing

When the laser intensity reaches $\sim 10^{14}\text{ W/cm}^2$, the collisional ionization increases the free electron density, which carry enough energy to promote material ablation after relaxation to the material ions and atoms. Due to the pulse interaction almost exclusively with electrons, the ultrashort pulses ablation threshold, F_{th} , is almost independent of the material characteristics (reflectivity, absorption, thermal conductivity, density), being related to the easiness (or difficulty) of creating the first free electrons that will initiate the avalanche. For this reason, the ablation threshold will depend on the material class (metal, semiconductor, dielectric), and on the presence of defects and impurities [51, 52] that create intermediate levels in the bandgap, decreasing the ionization threshold. These defects can be intrinsic to the material, or created by the laser, such as color centers [46] that increase the pulse absorption. In this case, when processing solids with superimposing pulses modifications can be induced in the material, lowering the F_{th} for subsequent pulses. These cumulative phenomena are known as incubation effects [53-55].

In 2006 we introduced a technique known as D-Scan (Diagonal-Scan) [56] to determine a material F_{th} for ultrashort pulses, in which a sample travels diagonally across the beamwaist of a focused laser beam, etching in its surface the profile shown in Fig. 4. Measuring half of the maximum transversal dimension of the profile, ρ_{max} , and knowing the laser pulse power P_0 immediately determines the ablation threshold by:

$$F_{th} = 0.117 P_0 / \rho_{max}^2. \quad (3)$$

To determine the number of superimposed pulses, N , that created the profile and defined F_{th} , a second expression is used [55]:

$$N = 1.8 (f \rho_{max}) / v_y, \quad (4)$$

where f is the pulses repetition rate and v_y is the sample transversal speed.

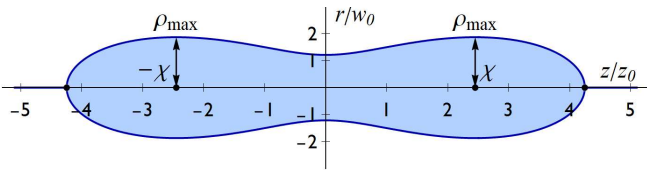


Fig. 4. D-Scan trace to determine a material F_{th} .

Performing a few scans at different v_y and f leads to the determination of the sample incubation parameter [53, 57], which quantifies how defects are accumulated. Using this method, we measure ablation threshold and incubation parameters for a variety of materials [58], including metals [59, 60], glasses and crystals [55, 61, 62], and used the results to texturize tools [63] and manufacture structures such as microfluidic circuits [64, 65], as the ones shown in Fig. 5.

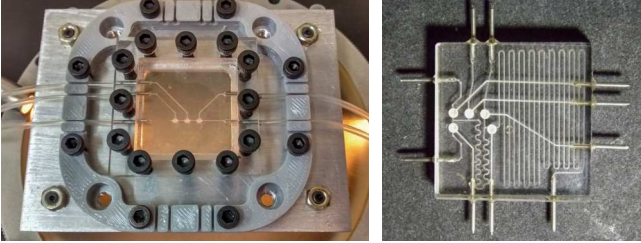


Fig. 5. Microfluidic circuits manufactured in BK7 glass by ultrashort laser pulses machining.

It is possible to finely tune the ablation characteristics by controlling the interaction parameters (pulse energy, focusing [66], pulses superposition), and process materials in very different ways, such as promoting phase transitions like converting amorphous graphite into diamond [67], and *in vivo* removing burned tissue from mammals skin [68, 69]. In this last case, the tissue recovering was similar to the obtained with traditional methods, with the advantage of minimized contamination due to the non-contact laser ablation process, and preservation of healthy tissue.

One additional advantage of the ultrashort pulses ablation is that they can be accompanied by the sample characterization provided by its plasma emission. The plasma emission lines can be used to determine the material elemental composition, and this technique, known as fs-LIBS, was applied to a variety of materials [70, 71] due to the nonselective interaction of the ultrashort pulses, allowing their composition mapping [72].

D. High Harmonics Generation

For pulses with intensities of $10^{14} - 10^{15}$ W/cm² impinging on a gas target, the freed electrons gain kinetic energy from the laser field, and when performing a closed trajectory emit it as photons when recombining with their parent atoms. Using Argon, we could generate up to the 21st harmonic of the laser, producing ~ 30 eV photons at ~ 40 nm [73, 74], and measure their divergence [75]. The harmonics can also be slightly tuned, depending on the exciting pulses dispersion, as shown in Fig. 6, which presents the harmonics intensity map dependence on the CPA compressor gratings position around the transform limited pulse ($\Delta x = 0$). For the transform limited pulse, each harmonic intensity has a minimum due to the high electronic density produced in the gas target, which reflects part of the pulse due to the plasma frequency approaching the laser frequency. As the pulse duration shortens for positive and negative dispersions, the harmonic intensity peaks and shifts its central wavelength.

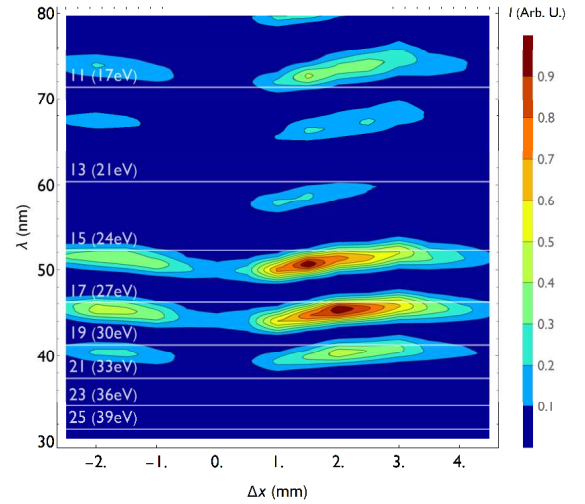


Fig. 6. HHG dependence on the pulse dispersion around the micrometer position ($\Delta x = 0$) that defines the transform limited pulse. The horizontal lines indicate the harmonic order based on the laser central wavelength.

E. Laser Particle Acceleration

More recently, we have been working towards the acceleration of electrons by ultrashort laser pulses, which requires laser intensities in the range $10^{16} - 10^{18}$ W/cm². As described in Section II, at this intensity interval the atomic potential binding electrons is severely distorted, and the electrons are ejected by BSI, creating a plasma through which the pulse propagates. Ponderomotive and nonlinear relativistic forces modulate the laser beam and reconfigure the electrons distribution, creating condition for electrons acceleration. We have been performing Particle-In-Cell (PIC) simulations [76], while working to upgrade our laser to reach the 1 TW region, providing incident intensities above 10^{16} W/cm², already obtained in our laboratories [77]. Our goal is to generate an electron beam with significant charge and energies of tens of MeV, at high repetition rates [78], to study its use in the production of radiopharmaceuticals for cancer treatment [79].

Fig. 7 shows the results for the simulation of a 2 TW peak power laser pulse propagating through a target composed by H₂ gas with 10^{20} atoms/cm³. The upper map shows the electronic density distribution on the laser polarization plane after the pulse propagated ~ 190 μ m inside the gas target. The wake follows the pulse, and ionic cavities (bubbles) can be clearly seen. The ponderomotive and electrostatic forces

accumulate the electrons at the bubbles extremities (~ 175 , ~ 179 and $\sim 187 \mu\text{m}$). The lower graph presents the electron density (blue) and the electric field originated by it (red), along the axis (dashed line in the map). The field amplitude reaches almost 100 GeV, and an electron bunch being accelerated can be identified at $\sim 182 \mu\text{m}$.

Configurations similar to this one are of interest to us, and we are proceeding with simulation studies to maximize the energy and charge of the generated bunches [78]. We are also working to upgrade our laser to a few TW peak power to be able to generate these electron bunches at the lab.

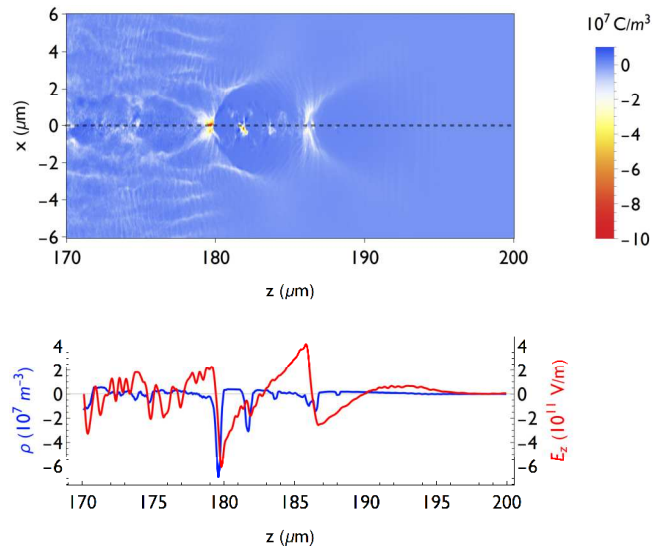


Fig. 7. (upper) charge density distribution created in the laser polarization plane by a 2 TW propagating in a 2×10^{20} H atoms/cm³. (bottom) charge density (blue) and electric field (red) on the axis of the upper graph.

V. CONCLUSIONS

We presented a review of the interaction of ultrashort laser pulses with matter, covering the applications that are being developed in our laboratory and presented results that were obtained there. Many other applications of ultrashort laser pulses exist, and are described by phenomena not discussed here, and we expect to have given a taste of the importance that these pulses exert on physics frontiers nowadays.

REFERENCES

- [1] P. F. Moulton, "Spectroscopic and laser characteristics of Ti:Al₂O₃," *J. Opt. Soc. Am. B*, vol. 3, pp. 125-133, 1986.
- [2] D. Strickland, and G. Mourou, "Compression of amplified chirped optical pulses," *Opt. Commun.*, vol. 56, pp. 219-221, 1985.
- [3] S. Backus, "Direct diode pumped Ti:sapphire ultrafast regenerative amplifier system," *Opt. Expr.*, vol. 25, pp. 3666-3674, 2017.
- [4] M. Muller, "10.4 kW coherently combined ultrafast fiber laser," *Opt. Lett.*, vol. 45, pp. 3083-3086, 2020.
- [5] J. Pupeikis, "Water window soft x-ray source enabled by a 25 W few-cycle 22 μm OPCPA at 100 kHz," *Optica*, vol. 7, pp. 168-171, 2020.
- [6] C. N. Danson, "Petawatt and exawatt class lasers worldwide," *High P. Las. Sci. Eng.*, vol. 7, p. E54, 2019.
- [7] S. Grundmann, "Zeptosecond birth time delay in molecular photoionization," *Science*, vol. 370, pp. 339-341, 2020.
- [8] J. B. Marion, and M. A. Heald, *Classical electromagnetic radiation*, 3rd ed. Victoria, Melbourne: Brooks/Cole, 1995.
- [9] R. W. Boyd, *Nonlinear optics*, 3rd ed. Boston: Academic Press, 2008.
- [10] A. Spott, A. Becker, and A. Jaroń-Becker, "Transition from perturbative to nonperturbative interaction in low-order-harmonic generation," *Phys. Rev. A*, vol. 91, p. 023402, 2015.

- [11] L. V. Keldysh, "Ionization in the Field of a Strong Electromagnetic Wave," *Sov. Phys. JETP-USSR*, vol. 20, pp. 1307-1314, 1965.
- [12] S. Augst, D. D. Meyerhofer, D. Strickland, and S. L. Chint, "Laser ionization of noble gases by Coulomb-barrier suppression," *J. Opt. Soc. Am. B*, vol. 8, pp. 858-867, 1991.
- [13] S. Nolte, "Ablation of metals by ultrashort laser pulses," *J. Opt. Soc. Am. B*, vol. 14, pp. 2716-2722, 1997.
- [14] B. C. Stuart, "Optical ablation by high-power short-pulse lasers," *J. Opt. Soc. Am. B*, vol. 13, pp. 459-468, 1996.
- [15] D. Du, X. Liu, G. Korn, J. Squier, and G. Mourou, "Laser-induced breakdown by impact ionization in SiO₂ with pulse widths from 7 ns to 150 fs," *Appl. Phys. Lett.*, vol. 64, pp. 3071-3073, 1994.
- [16] N. Bloembergen, "Laser-Induced Electric Breakdown in Solids," *IEEE J. Quantum Elec.*, vol. QE10, pp. 375-386, 1974.
- [17] E. G. Gamaly, A. V. Rode, V. T. Tikhonchuk, and B. Luther-Davies, "Electrostatic mechanism of ablation by femtosecond lasers," *Appl. Surf. Sci.*, vol. 197-198, pp. 699-704, 2002.
- [18] N. M. Bulgakova, and I. M. Bourakov, "Phase explosion under ultrashort pulsed laser ablation: modeling with analysis of metastable state of melt," *Appl. Surf. Sci.*, vol. 197, pp. 41-44, 2002.
- [19] P. Lorazo, L. Lewis, and M. Meunier, "Short-Pulse Laser Ablation of Solids: From Phase Explosion to Fragmentation," *Phys. Rev. Lett.*, vol. 91, p. 225502, 2003.
- [20] M. D. Perry, "Ultrashort-pulse laser machining of dielectric materials," *J. Appl. Phys.*, vol. 85, pp. 6803-6810, 1999.
- [21] J. Neev, "Ultrashort pulse lasers for hard tissue ablation," *IEEE J. Sel. Top. Quantum Elec.*, vol. 2, pp. 790-800, 1996.
- [22] L. T. Canguero, R. Vilar, A. M. Botelho do Rego, and V. S. Muralha, "Femtosecond laser ablation of bovine cortical bone," *J. Biomed. Opt.*, vol. 17, p. 125005, 2012.
- [23] D. von der Linde, and H. Schüller, "Breakdown threshold and plasma formation in femtosecond laser-solid interaction," *J. Opt. Soc. Am. B*, vol. 13, pp. 216-222, 1996.
- [24] A. J. Bauer, and S. G. Buckley, "Novel Applications of Laser-Induced Breakdown Spectroscopy," *Appl. Spectrosc.*, vol. 71, pp. 553-566, 2017.
- [25] P. Rohwetter, "Remote LIBS with ultrashort pulses: characteristics in picosecond and femtosecond regimes," *J. Anal. At. Spectrom.*, vol. 19, pp. 437-444, 2004.
- [26] M. Lewenstein, P. Balcou, M. Y. Ivanov, A. Lhuillier, and P. B. Corkum, "Theory of High-Harmonic Generation by Low-Frequency Laser Fields," *Phys. Rev. A*, vol. 49, pp. 2117-2132, 1994.
- [27] T. Popmintchev, M.-C. Chen, P. Arpin, M. M. Murnane, and H. C. Kapteyn, "The attosecond nonlinear optics of bright coherent X-ray generation," *Nat. Photonics*, vol. 4, pp. 822-832, 2010.
- [28] A. McPherson, "Studies of multiphoton production of vacuum-ultraviolet radiation in the rare gases," *J. Opt. Soc. Am. B*, vol. 4, pp. 595-601, 1987.
- [29] T. Popmintchev, "Bright Coherent Ultrahigh Harmonics in the keV X-ray Regime from Mid-Infrared Femtosecond Lasers," *Science*, vol. 336, pp. 1287-1291, 2012.
- [30] R. Bartels, "Shaped-pulse optimization of coherent emission of high-harmonic soft X-rays," *Nature*, vol. 406, pp. 164-166, 2000.
- [31] G. Sansone, "Isolated single-cycle attosecond pulses," *Science*, vol. 314, pp. 443-446, 2006.
- [32] https://en.wikipedia.org/w/index.php?title=Ponderomotive_force&oldid=1007462739, accessed 15-April-2021, 2021.
- [33] G. A. Mourou, "Ultraintense lasers: relativistic nonlinear optics and applications," *CR. Acad. Sci IV-Phys*, vol. 2, pp. 1407-1414, 2001.
- [34] D. Umstadter, "Review of physics and applications of relativistic plasmas driven by ultra-intense lasers," *Phys. Plasmas*, vol. 8, pp. 1774-1785, 2001.
- [35] E. Esarey, C. B. Schroeder, and W. P. Leemans, "Physics of laser-driven plasma-based electron accelerators," *Rev. Mod. Phys.*, vol. 81, pp. 1229-1285, 2009.
- [36] W. P. Leemans, "GeV electron beams from a centimetre-scale accelerator," *Nat. Phys.*, vol. 2, pp. 696-699, 2006.
- [37] J. Faure, "A review of recent progress on laser-plasma acceleration at kHz repetition rate," *Plasma Phys. Contr. Fus.*, vol. 61, p. 014012, 2019.

- [38] R. E. Samad, G. E. C. Nogueira, S. L. Baldochi, and N. D. Vieira, "Development of a flashlamp-pumped Cr:LiSAF laser operating at 30 Hz," *Appl. Opt.*, vol. 45, pp. 3356-3360, 2006.
- [39] R. E. Samad, S. L. Baldochi, G. E. C. Nogueira, and N. D. Vieira, "30 W Cr:LiSrAlF₆ flashlamp-pumped pulsed laser," *Opt. Lett.*, vol. 32, pp. 50-52, 2007.
- [40] R. E. Samad, G. E. C. Nogueira, S. L. Baldochi, and N. D. Vieira, "5 Hz flashlamp pumped Cr:LiSAF multipass amplifier for ultrashort pulses," *J. Opt. A: Pure Appl. Opt.*, vol. 10, p. 104010, 2008.
- [41] R. Szipocs, K. Ferencz, C. Spielmann, and F. Krausz, "Chirped multilayer coatings for broadband dispersion control in femtosecond lasers," *Opt. Lett.*, vol. 19, pp. 201-203, 1994.
- [42] D. J. Jones, "Carrier-envelope phase control of femtosecond mode-locked lasers and direct optical frequency synthesis," *Science*, vol. 288, pp. 635-640, 2000.
- [43] G. P. Agrawal, and N. A. Olsson, "Self-phase modulation and spectral broadening of optical pulses in semiconductor laser amplifiers," *IEEE J. Quantum Elec.*, vol. 25, pp. 2297-2306, 1989.
- [44] R. H. Stolen, and C. Lin, "Self-phase-modulation in silica optical fibers," *Phys. Rev. A*, vol. 17, pp. 1448-1453, 1978.
- [45] J. H. Sierra, "Low-loss pedestal Ta₂O₅ nonlinear optical waveguides," *Opt. Expr.*, vol. 27, pp. 37516-37521, 2019.
- [46] L. C. Courrol, "Color center production by femtosecond pulse laser irradiation in LiF crystals," *Opt. Expr.*, vol. 12, pp. 288-293, 2004.
- [47] L. C. Courrol, "Study of color centers produced in thulium doped YLF crystals irradiated by electron beam and femtosecond laser pulses," *Opt. Commun.*, vol. 270, pp. 340-346, 2007.
- [48] L. C. Courrol, "Stabilized color centers created by high-intensity ultrashort pulse laser in pure YLF crystals," *J. Lumin.*, vol. 122, pp. 318-321, 2007.
- [49] J. D. Jackson, *Classical electrodynamics*, 3rd ed. New York: Wiley, 1999.
- [50] D. S. da Silva, N. U. Wetter, W. de Rossi, L. R. P. Kassab, and R. E. Samad, "Production and characterization of femtosecond laser-written double line waveguides in heavy metal oxide glasses," *Opt. Mat.*, vol. 75, pp. 267-273, 2018.
- [51] F. Costache, S. Eckert, and J. Reif, "Near-damage threshold femtosecond laser irradiation of dielectric surfaces: desorbed ion kinetics and defect dynamics," *Appl. Phys. A-Mat. Sci. Proc.*, vol. 92, pp. 897-902, 2008.
- [52] M. Mero, J. Liu, W. Rudolph, D. Ristau, and K. Starke, "Scaling laws of femtosecond laser pulse induced breakdown in oxide films," *Phys. Rev. B*, vol. 71, p. 115109, 2005.
- [53] D. Ashkenasi, M. Lorenz, R. Stoian, and A. Rosenfeld, "Surface damage threshold and structuring of dielectrics using femtosecond laser pulses: the role of incubation," *Appl. Surf. Sci.*, vol. 150, pp. 101-106, 1999.
- [54] J. Byskov-Nielsen, J.-M. Savolainen, M. S. Christensen, and P. Balling, "Ultra-short pulse laser ablation of metals: threshold fluence, incubation coefficient and ablation rates," *Appl. Phys. A-Mat. Sci. Proc.*, vol. 101, pp. 97-101, 2010.
- [55] L. M. Machado, R. E. Samad, W. de Rossi, and N. D. Vieira, "D-Scan measurement of ablation threshold incubation effects for ultrashort laser pulses," *Opt. Expr.*, vol. 20, pp. 4114-4123, 2012.
- [56] R. E. Samad, and N. D. Vieira, "Geometrical method for determining the surface damage threshold for femtosecond laser pulses," *Las. Phys.*, vol. 16, pp. 336-339, 2006.
- [57] Y. Jee, M. F. Becker, and R. M. Walsler, "Laser-Induced Damage on Single-Crystal Metal-Surfaces," *Journal of the Optical Society of America B-Optical Physics*, vol. 5, pp. 648-659, 1988.
- [58] R. E. Samad, F. C. Maia, N. M. Souza, W. de Rossi, and N. D. Vieira, "Determination of the Graphite Incubation Parameter in the Ultrafast Regime using the D-Scan Technique," in *Frontiers in Optics 2014*, Tucson, Arizona, 2014, p. LTh41.6.
- [59] R. E. Samad, D. C. Mirim, W. de Rossi, and N. D. Vieira, "Determination of the AISI 1045 steel ablation threshold dependence on the pulse superposition using the Diagonal Scan (D-Scan) technique," in *Frontiers in Ultrafast Optics: Biomedical, Scientific, and Industrial Applications XIV*, San Francisco, USA, 2014, p. 89721G.
- [60] E. S. Oliveira, R. E. Samad, N. D. Vieira, and W. d. Rossi, "Selective ablation of titanium nitride film on tungsten carbide substrate using ultrashort laser pulses," in *Lasers in Manufacturing Conference - LiM 2017*, 2017.
- [61] W. de Rossi, L. M. Machado, N. D. Vieira, and R. E. Samad, "D-Scan Measurement of the Ablation Threshold and Incubation Parameter of Optical Materials in the Ultrafast Regime," *Phys. Procedia*, vol. 39, pp. 642-649, 2012.
- [62] R. E. Samad, L. M. Machado, W. d. Rossi, and N. D. Vieira, "D-Scan Measurement of the Ablation Threshold and Incubation Parameter of Optical Materials in the Ultrafast Regime," in *Latin American Optics & Photonics 2012*, São Sebastião, Brazil, 2012, p. LT2A.1.
- [63] M. Bertolete, "Effects of texturing the rake surfaces of cemented tungsten carbide tools by ultrashort laser pulses in machining of martensitic stainless steel," *Int. J. Adv. Manuf. Tech.*, vol. 98, pp. 2653-2664, 2018.
- [64] L. M. Machado, R. E. Samad, A. Z. Freitas, N. D. Vieira, and W. de Rossi, "Microchannels Direct Machining using the Femtosecond Smooth Ablation Method," *Phys. Procedia*, vol. 12, pp. 67-75, 2011.
- [65] L. R. De Pretto, R. E. Samad, W. de Rossi, and A. Z. de Freitas, "Optical coherence tomography characterization of femtosecond laser manufactured microfluidic circuits," in *Microfluidics, BioMEMS, and Medical Microsystems XVI*, 2018, p. 104911A.
- [66] M. P. Raelle, L. R. De Pretto, W. de Rossi, N. D. Vieira, and R. E. Samad, "Focus Tracking System for Femtosecond Laser Machining using Low Coherence Interferometry," *Sci. Rep.*, vol. 9, p. 4167, 2019.
- [67] F. C. B. Maia, "Synthesis of diamond-like phase from graphite by ultrafast laser driven dynamical compression," *Sci. Rep.*, vol. 5, p. 11812, 2015.
- [68] M. O. d. Santos, "Imaging of nonlinear microscopy of burned skin treated by ultra-high intensity laser pulses," *Biomedical Spectroscopy and Imaging*, vol. 3, pp. 293-300, 2014.
- [69] M. O. D. Santos, "Multimodal evaluation of ultra-short laser pulses treatment for skin burn injuries," *Biomed. Opt. Express.*, vol. 8, pp. 1575-1588, 2017.
- [70] D. Santos Jr, "Temporal Evaluation of Femtosecond Laser Induced Plasma for Analysis of Soils by LIBS," in *4th International Conference on Laser Induced Plasma Spectroscopy and Applications*, Montreals, 2006.
- [71] D. Santos, "Evaluation of Femtosecond Laser-Induced Breakdown Spectroscopy for Analysis of Animal Tissues," *Appl. Spectrosc.*, vol. 62, pp. 1137-1143, 2008.
- [72] L. T. Bello, "Mercury Amalgam Diffusion in Human Teeth Probed Using Femtosecond LIBS," *Appl. Spectrosc.*, vol. 71, pp. 659-669, 2017.
- [73] R. Qindeel, "Influence of Gas Pressure on High Harmonic Generation on Argon," in *Latin American Optics & Photonics 2012*, Maresias Beach Hotel, São Sebastião, SP, Brazil: Optical Society of America, Washington, DC, 2012, pp. LM4A.2.
- [74] R. Qindeel, "Harmonic Generation in Argon by Femtosecond Ti:Sapphire Laser," in *X-Ray Lasers 2012*, Sebban, S., Gautier, J., Ros, D. and Zeitoun, P. Eds. Paris, France: Springer International Publishing, 2014, pp. 209-213.
- [75] A. A. Almeida, A. V. F. Zuffi, P. S. F. d. Matos, N. D. Vieira, and R. E. Samad, "Harmonics Beams Characterization Using the Knife-Edge Technique," in *High-Brightness Sources and Light-Driven Interactions*, Long Beach, CA, USA, 2016, p. ET4A.1.
- [76] E. P. Maldonado, R. E. Samad, A. V. F. Zuffi, F. B. D. Tabacow, and N. D. Vieira, "Self-modulated laser-plasma acceleration in a H₂ gas target, simulated in a spectral particle-in-cell algorithm: wakefield and electron bunch properties," in *2019 SBFoton International Optics and Photonics Conference*, São Paulo, Brazil, 2019, pp. 1-5.
- [77] R. E. Samad, A. V. F. Zuffi, E. P. Maldonado, and N. D. Vieira, "Development and Optical Characterization of Supersonic Gas Targets for High-Intensity Laser Plasma Studies," in *2018 SBFoton International Optics and Photonics Conference*, Campinas, Brazil, 2018, pp. 1-5.
- [78] E. P. Maldonado, "Electron beam properties in self-modulated laser wakefield acceleration using TW and sub-TW pulses," in *2021 SBFoton International Optics and Photonics Conference (SBFoton IOPC)*, in press.
- [79] N. D. Vieira, "Laser wakefield electron accelerator: possible use for radioisotope production," in *2021 SBFoton International Optics and Photonics Conference (SBFoton IOPC)*, in press